

Crossed-Beam Investigation of  $O(^3P) + C_2H_5 \rightarrow C_2H_4 + OH^\dagger$ 

Yong-Pal Park, Kyoo-Weon Kang, Se-Hee Jung, and Jong-Ho Choi\*

Department of Chemistry and Center for Electro- and Photo-Responsive Molecules, Korea University, 1, Anam-dong, Seoul 136-701, Korea

Received: November 7, 2009; Revised Manuscript Received: February 4, 2010

The reaction dynamics of ground-state atomic oxygen [ $O(^3P)$ ] with an ethyl radical ( $C_2H_5$ ) in the gas phase was investigated using high-resolution laser spectroscopy in a crossed-beam configuration. An exothermic channel of  $O(^3P) + C_2H_5 \rightarrow C_2H_4 + OH$  was identified, and the nascent distributions of OH ( $X^2\Pi: v'' = 0, 1$ ) showed significant internal excitations with an unusual bimodal feature of low and high rotational  $N''$ -components with neither spin-orbit nor  $\Lambda$ -doublet propensities. On the basis of the ab initio and statistical calculations, the reaction mechanism can be rationalized by two competing mechanisms: abstraction vs addition. The low  $N''$ -components with significant vibrational excitation can be described in terms of the direct abstraction process as a major channel. The extraordinarily hot rotational distribution of high  $N''$ -components implies that a portion of the fraction proceeds through the indirect short-lived addition-complex forming process. From the comparative analysis of the reactions of  $O(^3P) +$  several hydrocarbon molecules and radicals, the reactivity and mechanistic characteristics of the title reaction are discussed.

## Introduction

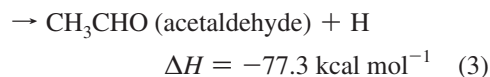
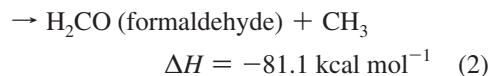
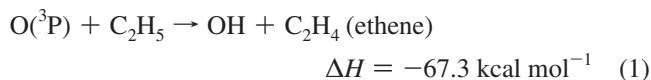
Gas-phase radical-radical reaction dynamics play a significant role in understanding the microscopic mechanisms of elementary reactive processes such as combustion, hydrocarbon synthesis, interstellar, and atmospheric chemistry. Despite their mechanistic significance, the studies of radical-radical reactive scattering at the molecular level, particularly in the field of reaction dynamics, are quite scarce compared to the more extensive atom-molecule reactions. Most of the gas-phase experimental investigations conducted thus far are related to bulk kinetics under thermally relaxed conditions. This dearth of a substantial body of investigation is primarily attributed to the difficulties in generating sufficient levels of clean hydrocarbon radicals and the realization of reliable and facile characterization schemes.<sup>1</sup>

In previous bimolecular reactive scattering experiments, Leone and co-workers studied the reactions of  $O(^3P)$  with ethyl radicals using time-resolved FT-IR spectroscopy and observed OH products.<sup>2</sup> Direct abstraction mechanism was proposed to explain the nonstatistical vibrational distributions of the OH products. Several groups performed kinetic investigations to obtain rate constants using mass spectrometry and laser spectroscopy.<sup>3</sup> Only a few theoretical studies have been reported on the title reaction. Harding and co-workers performed quantum chemical and classical trajectory calculations in an attempt to obtain high-pressure recombination rate constants.<sup>4</sup> Gupta et al. and Yang et al. carried out independent ab initio calculations on several reaction channels of  $O(^3P) + C_2H_5$ .<sup>5</sup>

In recent years this lab has performed combined crossed-beam and theoretical investigations into the reactions of  $O(^3P)$  with a series of prototypical hydrocarbon radicals, including allyl ( $C_3H_5$ ), propargyl ( $C_3H_3$ ), and *tert*-butyl ( $t-C_4H_9$ ), which show some intrinsic stability owing to resonance stabilization or hyperconjugation.<sup>1,6</sup> Leonori et al. also studied the oxidation

reaction of allyl radicals by means of the crossed-beam apparatus.<sup>7</sup> A supersonic flash pyrolysis source was adopted, where the labile precursor molecules underwent a rapid thermal decomposition to produce clean, jet-cooled radical beams without recombination and/or secondary dissociation.<sup>8</sup> With the aid of the ab initio calculations, the analyses of the nascent-state distributions of various reaction products have demonstrated unusual reactivity and mechanistic characteristics not previously observed in the reactions of  $O(^3P) +$  closed-shell hydrocarbon molecules.<sup>9</sup>

This work aims to provide our gas-phase crossed-beam investigation of the reaction dynamics of atomic oxygen  $O(^3P)$  with an ethyl radical ( $C_2H_5$ ). Apart from the fundamental importance in elementary reactive scattering processes, the oxidation reaction of ethyl radicals has been known as an important pathway under lean fuel conditions. The  $C_2H_5$  radical was produced by supersonic flash pyrolysis of the synthesized precursor azoethane ( $C_2H_5-N_2-C_2H_5$ ) that underwent a rapid thermal decomposition inside a high-temperature tube. The probed channel was the exothermic pathway (1) that produced a diatomic product OH and a closed-shell molecule ethene:



The reaction enthalpy was determined using the ab initio heat of formation.<sup>10</sup> On the other hand, in the previous mass-spectrometry experiments for reaction channels 1–3, a second-order rate constant and relative branching fractions over the temperature range of 295–600 K were determined to be  $(2.2 \pm 0.4) \times 10^{-10} \text{ cm}^3 \text{ molecule}^{-1} \text{ s}^{-1}$  and  $k_1:k_2:k_3 = 0.23:0.32:$

<sup>†</sup> Part of the special section "30th Free Radical Symposium".

\* Corresponding author. Tel: +82-2-3290-3135. Fax: +82-2-3290-3121. E-mail: jhc@korea.ac.kr.

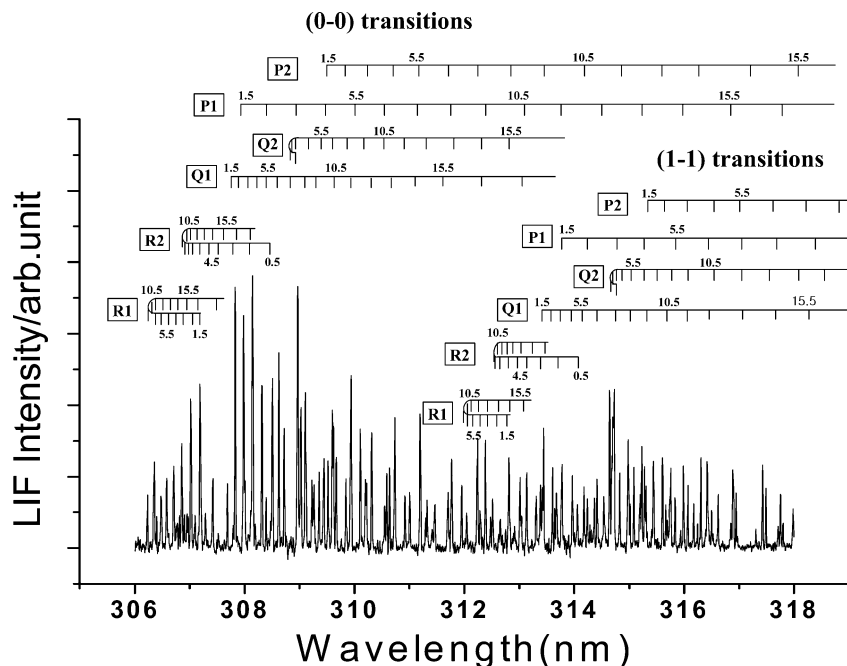


**Figure 1.** LIF spectrum in the 0–0 and 1–1 band regions of the nascent OH ( $A^2\Sigma^+ \rightarrow X^2\Pi$ ) produced from the reaction of  $O(^3P) + C_2H_5 \rightarrow OH + C_2H_4$ .

0.40, respectively.<sup>3</sup> The high reaction rate suggests that the title reaction proceeds through fast and irreversible association-fragmentation mechanisms.

In the presented crossed-beam scattering experiments, high-resolution laser-induced fluorescence (LIF) spectroscopy was employed to interrogate the nascent rovibrational distributions of the OH products from channel 1. Ab initio calculations using the density functional method were also performed, along with a complete basis model to elucidate the reaction mechanisms, kinetics, and dynamic characteristics of the title oxidation reaction. To the best of the authors' knowledge, no gas-phase crossed-beam study of the  $O(^3P) + C_2H_5$  reaction has been reported thus far. Therefore, the crossed-beam investigation presented herein can provide significant mechanistic insights into the oxidation reaction dynamics of saturated hydrocarbon radicals as a model system at the molecular level.

### Experiment and Ab Initio Calculations

The homemade crossed molecular beam apparatus designed for the presented investigations of reactive scattering was described in detail elsewhere.<sup>6</sup> Briefly, the apparatus consisted of two source chambers and a scattering chamber that were pumped by two 6 in. and one 10 in. baffled diffusion pumps, respectively. For generation of  $O(^3P)$ , 12%  $NO_2$  samples seeded in ultrahigh purity helium (UHP He: 99.999%) at a 2 atm stagnation pressure were expanded through a piezoelectrically actuated pulsed valve and irradiated by ca. 30 mJ pulses of the 355 nm laser beam near the throat of supersonic expansion. The  $C_2H_5$  radical was produced by supersonic flash pyrolysis of the precursor azoethane ( $C_2H_5-N_2-C_2H_5$ ). The azoethane was synthesized using the method of Renaud and Leitch.<sup>11</sup> The precursor seeded in the UHP He at 2 atm was completely pyrolyzed into  $C_2H_5$  and  $N_2$  inside a hot silicon carbide tube. At the center of the scattering chamber, both supersonic radical beams were crossed at right angles under the single collision condition. Assuming the full expansion of the molecular beams under the crossed-beam conditions,  $E_{com}$  was assessed to be 5.2 kcal mol<sup>-1</sup>. The nascent internal distributions of OH products

were examined using the LIF scheme of the (0,0) and (1,1) diagonal bands of the  $A^2\Sigma^+ \rightarrow X^2\Pi$  electronic transition in the 306–318 nm region. The resulting fluorescence was collected by a photomultiplier tube interfaced to a Boxcar signal averager and an IBM-PC for display and analysis. The minor interfering background signal resulting from the photolysis of the HONO impurity was subtracted to obtain the OH signal due solely to the title reaction.

Ab initio calculations on the title reaction conducted in this laboratory have been recently reported in detail elsewhere.<sup>10</sup> Here, a brief account necessary to help characterize the mechanistic pathways and the nascent population analysis of the observed OH products is presented. All calculations were performed using the Gaussian 03 system of programs on an IBM-PC and Compaq-Workstation (XP-1000).<sup>12–14</sup> Various geometries of local minima and transition states along the reaction coordinates were performed using the density functional method and the complete basis set models of CBS-Q and CBS-QB3, employing the 6-311G(d) and 6-311+G(3df,2p) basis sets. Unless otherwise specified, the single-point energies computed at the CBS-QB3 levels are presented in the discussion below. In addition, the vibration frequencies were also computed to characterize the stationary points and zero-point energy (ZPE) corrections with a scaling factor of 0.98. Here, it should be mentioned that Gupta et al. and Yang et al. also carried out independent ab initio calculations on a few reaction channels of  $O(^3P) + C_2H_5$  using Gaussian programs.<sup>5</sup> However, compared to those results, our extensive calculations demonstrated that our estimated heats of formation and reaction enthalpies correlated strongly with the known experimental values within an accuracy of <1.5 kcal mol<sup>-1</sup>.<sup>10</sup>

### Experimental Results

Figure 1 displays a typical LIF spectrum of the nascent OH ( $X^2\Pi: v'' = 0, 1$ ) products from the title reaction, together with the spectral assignment of individual lines. The assignment was performed by comparison with previously known line positions and further confirmed by spectral simulations.<sup>15</sup> The

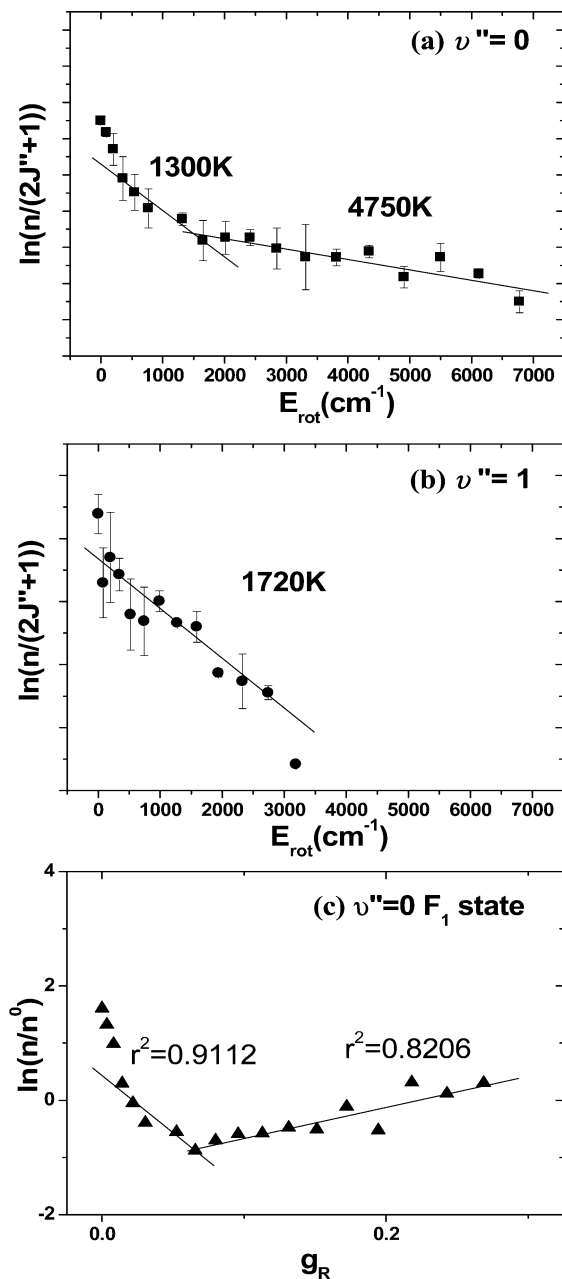


**Figure 2.** Boltzmann plots of the nascent OH distributions as a function of rotational energy for the  $F_1$  states of the (a)  $v'' = 0$  (■) and (b)  $v'' = 1$  (●) vibrational levels. (c) A rotational surprisal plot for the nascent OH produced in the reaction of  $O(^3P)$  with the ethyl radical for the  $F_1$  state of the  $v'' = 0$  vibrational level.

spectrum clearly demonstrates that the nascent products exhibit substantial rotational excitation in the observed  $v'' = 0$  and 1 vibrational states. Figure 2 displays the logarithmic plots of the populations divided by the rotational degeneracy as a function of rotational energy for the  $F_1$  ( $^2\Pi_{3/2}$ ) spin-orbit state in the  $v'' = 0$  and 1 levels. The plots show bimodal features composed of low- and high- $N''$  rotational components in each vibrational state. The feature is more obviously exhibited in the  $v'' = 0$  level, where the fraction of the rotational energy from the total available energy was higher. When a simple Boltzmann distribution is assumed for low- and high- $N''$  components, the slopes in Figure 2 correspond to rotational temperatures. For the  $v'' = 0$  level, the rotational temperatures were estimated to be 1300 K ( $F_1: ^2\Pi_{3/2}$ ) and 1010 K ( $F_2: ^2\Pi_{1/2}$ ) for low- $N''$  components, and 4750 K ( $F_1$ ) and 4760 K ( $F_2$ ) for high- $N''$

components. However, for the  $v'' = 1$  level, the rotational temperatures were found to be 1720 K ( $F_1$ ) and 1660 K ( $F_2$ ) for the low- $N''$  components. The temperatures for high- $N''$  components were not estimated due to the limited number of available populations in the probed distributions. In addition, all of the rotational populations for the individual branches were summed up, corrected, and compared to obtain the ratio of vibrational partitioning ( $P_{v''=0}:P_{v''=1}$ ). The corrections considered in the analysis were Franck-Condon factors (0.90 and 0.71 for the (0,0) and (1,1) bands, respectively) and the lifetime differences (686.0 ns for  $v' = 0$  and 748.4 ns for  $v' = 1$ ). The averaged vibrational partitioning with respect to the low- $N'' = 0$  level showed population inversion with a ratio of  $P_0:P_1 = 1:1.06 \pm 0.44$  and were found to be almost the same in the two spin-orbit states. The relative rotational populations for the two spin-orbit electronic states and the  $\Lambda$ -doublet propensity were also examined. No significant spin-orbit preferences were observed in each vibrational state ( $1.08 \pm 0.31$  and  $1.34 \pm 0.41$  for  $v'' = 0$  and 1, respectively). The  $\Lambda$ -doublet propensity was determined to be  $0.97 \pm 0.46$  for the  $v'' = 0$  level and  $1.11 \pm 0.29$  for the  $v'' = 1$  level, thereby implying no noticeable propensity.

## Discussion

The detailed mechanistic pathways that account for the observed bimodal rotational distributions and the inversion of vibrational populations of the OH products can be obtained from ab initio calculations. Figure 3 illustrates the schematic diagram of two competing reaction pathways on the lowest doublet potential energy surface: abstraction and addition. It is obvious that the facile abstraction process is the direct H-atom abstraction from the methyl group. The entrance barrier along the coordinate of abstraction reaction was predicted to be negligible. Such absence of an activation barrier can be attributed to the unusually small C-H bond dissociation energy (BDE = 36.2 kcal mol<sup>-1</sup>) and the high reaction exothermicity of -67.3 kcal mol<sup>-1</sup>. Here, the H-atom abstraction from the CH<sub>2</sub> group of C<sub>2</sub>H<sub>5</sub> was not taken into account due to unfavorable endothermic reaction pathways to the formation of OH + <sup>1</sup>CH<sub>3</sub>CH and <sup>3</sup>CH<sub>3</sub>CH ( $\Delta H = 8.0$  and 5.6 kcal mol<sup>-1</sup>, respectively). Similar barrierless systems can be found in the H-atom abstraction reactions of  $O(^3P) +$  allyl and *tert*-butyl radicals, where the absence was also attributed to the unusually small C-H bond dissociation energy (BDE = 57.6 and 35.5 kcal mol<sup>-1</sup> for allyl and *tert*-butyl, respectively) and the high reaction exothermicities ( $\Delta H = -46.0$  and  $-67.2$  kcal mol<sup>-1</sup> for allyl and *tert*-butyl, respectively).<sup>6</sup> The absence is well compared with the substantial barriers existing in the abstraction reactions of  $O(^3P)$  with CH<sub>3</sub>, C<sub>3</sub>H<sub>3</sub>, and closed-shell hydrocarbon molecules, where the large C-H BDE and unfavorable reaction exothermicities entail overcoming the high activation barriers along the reaction coordinates.<sup>6,9,10</sup>

A second pathway to the formation of C<sub>2</sub>H<sub>4</sub> + OH is predicted to be the indirect addition reaction, a characteristic barrierless process of the title radical-radical reaction. As atomic oxygen attacks C<sub>2</sub>H<sub>5</sub> along the entrance reaction coordinate, the strong, long-range attractive interaction between the two open-shell radicals leads to an energized C<sub>2</sub>H<sub>5</sub>O intermediate denoted as eINT1 in Figure 3, with a high association exothermicity of -92.7 kcal/mol with respect to the reactant radicals. Due to the plentiful internal energy, eINT1 can undergo further isomerization steps, resulting in the formation of another two energized isomers, eINT2 and eINT3: the eINT1 might undergo H-atom migration from either C(1) or

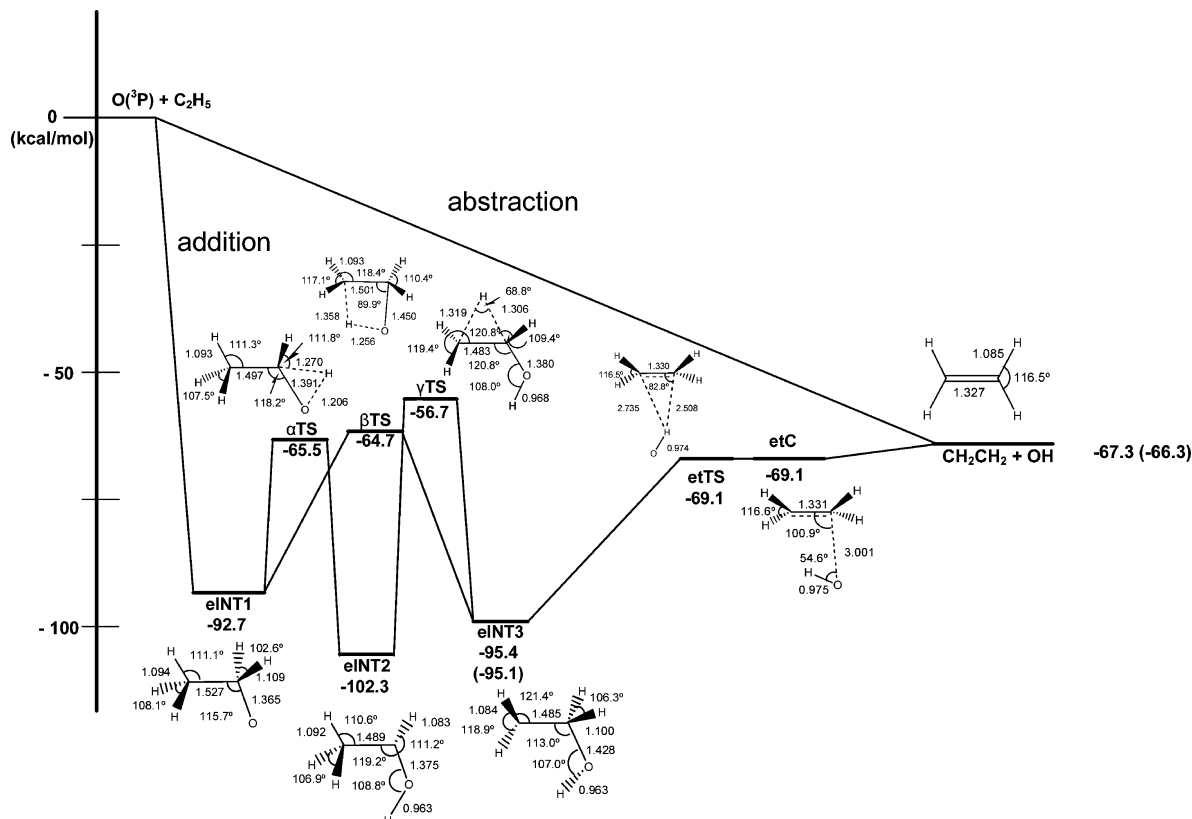


**Figure 3.** Schematic energy diagram of the potential energy surface with the optimized geometries along the  $\text{O}(^3\text{P}) + \text{C}_2\text{H}_5 \rightarrow \text{OH} + \text{C}_2\text{H}_4$  reaction coordinate at the CBS-QB3 level of theory. Values in parentheses denote experimental values ( $\text{kcal mol}^{-1}$ ).

$\text{C}(2)$  to the oxygen atom to form eINT2 ( $\text{CH}_3\text{CHOH}$ ) and eINT3 ( $\text{CH}_2\text{CH}_2\text{OH}$ ) by overcoming the respective three- and four-membered transition states ( $\alpha\text{TS}$  and  $\beta\text{TS}$ ). The activation barriers were calculated to be 27.2 and 28.0  $\text{kcal mol}^{-1}$ , respectively, and belong in the typical range 20–40  $\text{kcal mol}^{-1}$  for the H-atom migration process. Here, it should be mentioned that eINT2 and eINT3 were calculated to be mutually convertible by overcoming the three-membered transition state ( $\gamma\text{TS}$ ) with a barrier height of 45.6  $\text{kcal mol}^{-1}$ . Finally, eINT3 undergoes a peculiar isomerization process leading to the title reaction pathway. After the direct  $\text{C}(1)\text{--OH}$  bond rupture through the eTTS transition state, the H atom of the OH radical is rotated toward  $\text{C}_2\text{H}_4$  to form the so-called van der Waals complex etC. The complex shows a weakly bound structure with  $C_s$  symmetry, in which the electron-deficient H atom of the OH radical perpendicularly interacts with the  $\pi$  bond of  $\text{C}_2\text{H}_4$ . The  $\text{OH}\cdots\text{C}$  bond length and stabilization energy with respect to the products ( $\text{C}_2\text{H}_4 + \text{OH}$ ) were estimated to be 2.508 Å and  $-1.8 \text{ kcal mol}^{-1}$ , respectively. The prediction is quite consistent with the recent theoretical studies on the reaction of ethylene + OH, in which as the OH radical approaches ethylene, the prereaction association adduct was predicted to exist along the entrance channel.<sup>16</sup>

The *prior* statistical theory and surprisal analysis based upon the aforementioned theoretical calculations were applied to characterize the observed nascent distributions.<sup>17,18</sup> For a decomposing energized intermediate such as eINT3, the statistical product-state distributions are assumed to be solely determined by the available phase space volumes of the two fragment products  $\text{C}_2\text{H}_4 + \text{OH}$ . In obtaining the rotational temperatures from the slopes, the very low- $N''$  regions were known to be very susceptible to the possible relaxation even under single-collision conditions.<sup>1,6</sup> Therefore, the lowest three points were

excluded in our analysis. Compared to the observed experimental distributions of the OH products at a collision energy of 5.2  $\text{kcal mol}^{-1}$ , the prior calculations predicted quite different rotational temperatures [2940 K ( $F_1$ ) and 2920 K ( $F_2$ ) for the  $v'' = 0$  level and 2650 K ( $F_1$ ) and 2630 K ( $F_2$ ) for the  $v'' = 1$  level] and a smaller fraction ( $P_1/P_0 = 0.20$ ) of population partitioned into  $v'' = 1$ . In addition, statistical surprisal analysis based upon the prior populations ( $n^0$ ) was also performed to deconvolute the observed bimodal rotational distributions ( $n$ ) of the  $v'' = 0$  level. The rotational surprisal analysis reveals the extent of the deviation from the statistical distribution and can be used to deduce the relative contribution. The surprisals,  $I(f_i/f_v) = -\ln[n(v'', J'')/n^0(v'', J'')]$  were plotted as a function of the rotational fraction of the available energy,  $g_R = f_i/(1 - f_v)$ , and shown in Figure 2c. Here,  $f_i$  and  $f_v$  are the fraction of the rotational and vibrational energy of the OH product, respectively. As shown in Figure 2c, it was not possible to deconvolute the rotational populations due to very poor fits except for the large negative slope in the low- $N''$  regime, suggesting that the low rotational components are highly populated in comparison to the expected statistical distribution. When the nascent distributions were simply deconvoluted, the approximate ratio of population partitioning for the low- and high- $N''$  components was estimated to be about 1.5: 1.

The discrepancy between the observed bimodal internal distributions and the *prior* distributions shows that the statistical picture is not sufficiently appropriate to describe the dynamical biases manifested in the title atom–radical reactive scattering processes. On the basis of both crossed-beam results and ab initio calculations, the reaction mechanism at the molecular level is believed to proceed through the following two competing dynamic pathways: abstraction vs addition. The low- $N''$  components with significant vibrational excitation can be described

in terms of the direct abstraction process as a major channel. Nevertheless, the minor but extraordinarily hot rotational distribution of high- $N''$  components implies that some fraction of the reactants proceeds through an indirect short-lived addition-complex forming process, such as eINT3. A similar abstraction mechanism was also proposed in the infrared emission study of OH produced in the reaction of  $O(^3P) + C_2H_5$  performed by Leone and co-workers.<sup>2</sup> Although clear rotational-state distribution in each vibrational state was not characterized due in part to the error (10–50%) associated with the each rotational level population, the inverted OH vibrational population was rationalized through a direct abstraction mechanism.

The competing reaction pathways of the title reaction stand in sharp contrast with the reaction mechanisms of  $O(^3P) +$  saturated hydrocarbon molecules and an unsaturated propargyl radical.<sup>6,9</sup> The former proceeds through the well-known collinear abstraction mechanism, producing the vibrationally hot and rotationally cold OH products. The latter, with the high entrance barrier, has only been described in terms of the addition pathway in the low collision energy regime. Similar reaction mechanisms have been observed in the reactions of  $O(^3P)$  with allyl ( $C_3H_5$ ) and *tert*-butyl ( $t-C_4H_9$ ), where both facile H-atom abstraction and barrierless addition pathways result in the formation of stable allene ( $C_3H_4$ ) and isobutene ( $i-C_4H_8$ ) + OH products.<sup>6</sup>

As demonstrated above, the work herein represents a step forward in understanding radical–radical reactions at the molecular level. Extensive crossed-beam investigations combined with *ab initio* calculations on several radical–radical reactions are currently being conducted. It is the hope of the authors that the gas-phase reaction dynamics studies presented herein will provide valuable mechanistic insights into the unexplored elementary oxidation reactions of various hydrocarbon radicals.

**Acknowledgment.** This work was supported by a National Research Foundation of Korea (NRF) grant funded by the Korea government (MEST) (No. M10500000023-06J0000). We thank Professor I. Fischer and Dr. B. Noller for their helpful discussion in synthesizing the precursor.

## References and Notes

- (1) Choi, J. H. *Int. Rev. Phys. Chem.* **2006**, *25*, 613.
- (2) Lindner, J.; Loomis, R. A.; Klaassen, J. J.; Leone, S. R. *J. Chem. Phys.* **1998**, *108*, 1944.
- (3) (a) Baulch, D. L.; Bowman, C. T.; Cobos, C. J.; Cox, R. A.; Just, Th.; Kerr, J. A.; Pilling, M. J.; Stocker, D.; Troe, J.; Tsang, W.; Walker, R. W.; Warnatz, J. *J. Phys. Chem. Ref. Data* **2005**, *34*, 757. (b) Slagle, I. R.; Sarzynski, D.; Gutman, D.; Miller, J. A.; Melius, C. F. *J. Chem. Soc., Faraday Trans. 2* **1988**, *84*, 49. (c) Hoyermann, K.; Olzmann, M.; Seeba, J.; Viskolcz, B. *J. Phys. Chem. A* **1999**, *103*, 5692. (d) Hack, W.; Hoyermann, K.; Olzmann, M.; Zeuch, T. *Proc. Combust. Institute* **2002**, *29*, 1247. (e) Reid, J. P.; Marcy, T. P.; Kuehn, S.; Leone, S. R. *J. Chem. Phys.* **2000**, *113*, 4572. (f) Herron, J. T. *J. Phys. Chem. Ref. Data* **1988**, *17*, 967.
- (4) Harding, L. B.; Klippenstein, S. J.; Georgievskii, Y. *Proc. Combust. Inst.* **2005**, *30*, 985.
- (5) (a) Yang, Y.; Weijun, Z.; Xiaoming, G.; Shixin, P.; Jie, S.; Wei, H.; Jun, Q. *Chinese J. Chem. Phys.* **2005**, *18*, 515. (b) Gupta, A.; Singh, R. P.; Singh, V. B.; Mishra, B. K.; Sathyamurthy, N. *J. Chem. Sci.* **2007**, *119*, 457.
- (6) (a) Kwon, H. C.; Park, J. H.; Lee, H.; Kim, H. K.; Choi, Y. S.; Choi, J. H. *J. Chem. Phys.* **2002**, *116*, 2675. (b) Park, J. H.; Lee, H.; Kwon, H. C.; Kim, H. K.; Choi, Y. S.; Choi, J. H. *J. Chem. Phys.* **2002**, *117*, 2017. (c) Lee, H.; Joo, S. K.; Kwon, L. K.; Choi, J. H. *J. Chem. Phys.* **2003**, *119*, 9337. (d) Lee, H.; Joo, S. K.; Kwon, L. K.; Choi, J. H. *J. Chem. Phys.* **2004**, *120*, 2215. (e) Joo, S. K.; Kwon, L. K.; Lee, H.; Choi, J. H. *J. Chem. Phys.* **2004**, *120*, 7976. (f) Nam, M. J.; Youn, S. E.; Li, L.; Choi, J. H. *J. Chem. Phys.* **2005**, *123*, 211105. (g) Choi, J. H.; Nam, M. J.; Youn, S. E. *ChemPhysChem* **2006**, *7*, 2526. (h) Lee, H.; Nam, M. J.; Choi, J. H. *J. Chem. Phys.* **2006**, *124*, 044311. (i) Park, J. H.; Lee, H.; Choi, J. H. *J. Chem. Phys.* **2003**, *119*, 8966.
- (7) Leonori, F.; Balucani, N.; Capozza, G.; Segoloni, E.; Stranges, D.; Casavecchia, P. *Phys. Chem. Chem. Phys.* **2007**, *9*, 1307.
- (8) Kohn, D. W.; Clauberg, H.; Chen, P. *Rev. Sci. Instrum.* **1992**, *63*, 4003.
- (9) (a) Kleimermanns, K.; Luntz, A. C. *J. Chem. Phys.* **1982**, *77*, 3533. (b) Andresen, P.; Luntz, A. C. *J. Chem. Phys.* **1980**, *72*, 5842.
- (10) Jung, S. H.; Park, Y. P.; Kang, K. W.; Choi, J. H. *J. Chem. Phys.*, submitted for publication.
- (11) Renaud, R.; Leitch, L. C. *Can. J. Chem.* **1954**, *32*, 545.
- (12) (a) Becke, A. D. *J. Chem. Phys.* **1992**, *96*, 2155. (b) Becke, A. D. *J. Chem. Phys.* **1993**, *96*, 1372. (c) Becke, A. D. *J. Chem. Phys.* **1993**, *98*, 5648.
- (13) Curtiss, L. A.; Raghavachari, K.; Redfern, P. C.; Pople, J. A. *J. Chem. Phys.* **1997**, *106*, 1063.
- (14) Frisch, M. J.; Trucks, G. W.; Schlegel, H. B.; Scuseria, G. E.; Robb, M. A.; Cheeseman, J. R.; Zakrzewski, V. G.; Montgomery, J. A., Jr.; Stratmann, R. E.; Burant, J. C.; Dapprich, S.; Millam, J. M.; Daniels, A. D.; Kudin, K. N.; Strain, M. C.; Farkas, O.; Tomasi, J.; Barone, V.; Cossi, M.; Cammi, R.; Mennucci, B.; Pomelli, C.; Adamo, C.; Clifford, S.; Ochterski, J.; Petersson, G. A.; Ayala, P. Y.; Cui, Q.; Morokuma, K.; Malick, D. K.; Rabuck, A. D.; Raghavachari, K.; Foresman, J. B.; Cioslowski, J.; Ortiz, J. V.; Baboul, A. G.; Stefanov, B. B.; Liu, G.; Liashenko, A.; Piskorz, P.; Komaromi, I.; Gomperts, R.; Martin, R. L.; Fox, D. J.; Keith, T.; Al-Laham, M. A.; Peng, C. Y.; Nanayakkara, A.; Gonzalez, C.; Challacombe, M.; Gill, P. M. W.; Johnson, B.; Chen, W.; Wong, M. W.; Andres, J. L.; Gonzalez, C.; Head-Gordon, M.; Replogle, E. S.; Pople, J. A. *Gaussian 03*; Gaussian, Inc.: Pittsburgh, PA, 2003.
- (15) (a) Dieke, G. H.; Crosswhite, H. M. *J. Quant. Spectrosc. Radiat. Transfer* **1962**, *2*, 97. (b) Dimpfl, W. L.; Kinsey, J. L. *J. Quant. Spectrosc. Radiat. Transfer* **1979**, *21*, 233. (c) Chidsey, I. L.; Crosley, D. R. *J. Quant. Spectrosc. Radiat. Transfer* **1980**, *23*, 187. (d) Luque, J.; Crosley, D. R. LIFBASE: Database and Simulation Program (v 2.0), SRI International Report MP 99-009, 1999.
- (16) (a) Zhu, R. S.; Park, J.; Lin, M. C. *Chem. Phys. Lett.* **2005**, *408*, 25. (b) Senosiain, J. P.; Klippenstein, S. J.; Miller, J. A. *J. Phys. Chem. A* **2006**, *110*, 6960. (c) Xu, Z. F.; Xu, K.; Lin, M. C. *ChemPhysChem* **2009**, *10*, 972.
- (17) Bear, T.; Hase, W. L. *Unimolecular Reactions Dynamics*; Oxford University Press: New York, 1996.
- (18) Holbrook, K. A.; Pilling, M. J.; Robertson, S. H. *Unimolecular Reactions*; John Wiley & Sons: New York, 1996.